Effects of dielectric confinement and electron-hole exchange interaction on excitonic states in semiconductor quantum dots

T. Takagahara
NTT Basic Research Laboratories, Musashino-shi, Tokyo 180, Japan
(Received 11 October 1991; revised manuscript received 29 July 1992)

A general scheme is established within the effective-mass approximation to calculate systematically the excitonic energy spectra in a semiconductor quantum dot including the dielectric confinement effect. This effect is found to appear most pronounced in the quantum-dot structure in comparison with the quantum-well and quantum-wire structures. A formula of the lowest exciton energy in the strong confinement regime is derived and the significance of the dielectric confinement effect is clarified. We investigate the dependence of the binding energy and the oscillator strength of the lowest-energy excitonic state on the quantum-dot radius, the electron-to-hole mass ratio, and the dielectric-constant ratio between the quantum dot and the surrounding medium. The subband mixing effect due to the electron-hole Coulomb interaction gives a finite oscillator strength to excitonic transitions which are forbidden in the absence of the Coulomb interaction. This effect is shown unambiguously in the calculated excitonic energy spectra. Furthermore, the electron-hole exchange interaction in a quantum dot is discussed. The short-range part of the exchange energy is shown to increase in proportion to the inverse of the volume of the quantum dot as the quantum-dot size is reduced. On the other hand, the long-range part of the exchange energy is found to be sensitively dependent on the shape of the quantum dot. In particular, it vanishes for the optically allowed excitonic states in a spherical quantum dot.

I. INTRODUCTION

Recently the low-dimensional semiconductor microstructures have been investigated extensively from the viewpoint of fundamental physics and from the interest for application to optical and electrical devices. The zero-dimensional microstructures which are usually called quantum dots or quantum boxes are now typically realized in semiconductor microcrystallites embedded in glasses[1,2] (colored glass filters) and in alkali halides[3] and are also fabricated by chemical methods,[4,5] by lithographic techniques[6–9] and by crystal growth methods.[10,11] The linear and nonlinear optical properties of these structures have been extensively investigated in recent years.[12–26] In these semiconductor microcrystallites, the carriers are confined three dimensionally and the translational symmetry is totally lost. This quantum confinement effect changes the energy-level continuum in the bulk material into a discrete level structure, namely, subband structure, and leads to the enhancement of the oscillator strength of excitons through the increased spatial overlap between an electron and a hole.[27,28] Another interesting property which will be manifested in low-dimensional structures is the dielectric confinement effect. Semiconductor microcrystallites are usually embedded within a material having a relatively small dielectric constant. The electric force lines emerging from charged particles within a semiconductor microcrystallite pass through the surrounding medium with a smaller dielectric constant than that of the semiconductor. Thus the screening effect is reduced and the Coulomb interaction between charged particles becomes enhanced, resulting in the enhancement of the exciton binding energy and the exciton oscillator strength. This dielectric confinement effect was first investigated by Keldysh[29] for a layered structure. Most recently we have studied this effect more thoroughly for the dielectric quantum-well (DQW) structure and clarified the enhancement of the exciton binding energy and the exciton oscillator strength.[30] A similar enhancement effect has been discussed for the quantum wire structure.[31,32] The dielectric confinement effect is expected to appear more pronounced in the quantum-dot structure than in quantum-well and quantum-wire structures because of more probable penetration of the electric force lines into the surrounding medium having a smaller dielectric constant. The critical size which characterizes the reduction in the dimensionality is of the order of the electron-hole separation, namely, the exciton Bohr radius. In a quantum dot whose size is of the same order as the exciton Bohr radius, an electron and a hole composing an exciton feel the dielectric boundary and their motions are strongly affected. On the other hand, when the quantum-dot size is much larger than this length scale, the situation is similar to that in the bulk medium and the dielectric confinement effect would not be effective.

As a consequence of these two effects, namely, the quantum confinement effect and the dielectric confinement effect, the electron-hole exchange interaction is also enhanced which gives the energy difference between the spin-singlet and -triplet excitons. As is well known, the long-range part of this interaction in the bulk material gives rise to the longitudinal-transverse (LT) splitting energy of excitons.[33] However, in semiconductor quantum dots the translational symmetry is totally absent and the long-range part of the electron-hole exchange interaction is expected to be sensitively dependent on the size and shape of the quantum dot.

In Sec. II, general aspects of the excitonic states in a spherical quantum dot are investigated within the effective-mass approximation. In Sec. III, the significant effect of the dielectric confinement on the exciton energy is clarified in the strong confinement regime and a new formula for the exciton energy is presented. In Sec. IV, a general scheme to calculate systematically the excited excitonic states is presented and several lowest excitonic states are determined by a variational method. In Secs. V and VI, the binding energy and the oscillator strength of the lowest exciton state are calculated as functions of the quantum-dot radius, the electron-to-hole mass ratio, and the dielectric-constant ratio between the semiconductor material and the surrounding medium. In these calculations, the significance of the dielectric confinement effect is demonstrated. In Sec. VII, the subband mixing effect due to the electron-hole Coulomb interaction is shown clearly in the calculated excitonic energy spectra. This mixing effect gives a finite oscillator strength to interband transitions which are forbidden in the absence of the Coulomb interaction. In Sec. VIII, the electron-hole exchange energy in a semiconductor quantum dot is discussed. The short-range part of the exchange energy is shown to increase in proportion to the inverse of the volume of a quantum dot as the quantum-dot size is reduced. On the other hand, the long-range part of the exchange energy is found to be sensitively dependent on the shape of the quantum dot and to vanish for the optically allowed excitonic states in a spherical quantum dot.

II. EXCITONIC STATES IN SEMICONDUCTOR QUANTUM DOTS

Here the general aspects of the ground and excited excitonic states in a spherical quantum dot will be discussed. Although many authors have discussed this subject,[34–42] the effect of the dielectric confinement on the excitonic states has not yet been clarified in detail. We will discuss the general aspects focusing our attention on the dielectric confinement effect. In the effective-mass approximation the relevant Hamiltonian for an electron-hole pair in a spherical quantum dot with radius R was derived by Brus[35] and is given as

$$H=-\frac{\hbar^2}{2m_e}\nabla_e^2-\frac{\hbar^2}{2m_h}\nabla_h^2-\frac{e^2}{\epsilon_1|r_e-r_h|}+\frac{e^2}{2R}\sum_{n=0}^{\infty}\alpha_n\left[\left(\frac{r_e}{R}\right)^{2n}+\left(\frac{r_h}{R}\right)^{2n}\right]-\frac{e^2}{R}\sum_{n=0}^{\infty}\alpha_n\left(\frac{r_e r_h}{R^2}\right)^n P_n(\cos\Theta_{eh}) , \tag{2.1}$$

where r_e and r_h denote the coordinates of an electron and a hole, respectively, m_e and m_h are their effective masses, P_n is the Legendre polynomial of the nth order, and Θ_{eh} is the angle between r_e and r_h. The dielectric constants of the semiconductor material and the surrounding medium are denoted by ϵ_1 and ϵ_2, respectively, and α_n is defined by

$$\alpha_n=\frac{(n+1)(\epsilon-1)}{\epsilon_1(n\epsilon+n+1)} , \tag{2.2}$$

with $\epsilon=\epsilon_1/\epsilon_2$. The first two terms in (2.1) represent the kinetic energy and the third term is the direct Coulomb interaction between an electron and a hole. The last two terms are usually called the surface polarization energy, which arises from the difference in the dielectric constant between the semiconductor quantum dot and the surrounding medium. The former is the self-energy of an electron and a hole due to its own image charge, whereas the latter is the mutual interaction energy between an electron and a hole via image charges. The expression of the dielectric confinement energy for an exciton is dependent on the shape of the quantum dot. The expression for a general cuboid is given in Appendix A for the sake of reference.

In calculating the exciton-energy spectra, the boundary conditions on the exciton wave function play an important role. In actual samples of quantum dots, e.g., semiconductor microcrystallites embedded in a glass matrix, the energy-gap difference between the semiconductor and the surrounding medium is rather large and at the same time the bonding characters of both materials are considerably different. Thus the potential discontinuity for the electron and the hole between the two materials is determined not only by the energy-gap difference but also by the surface potential. At present our knowledge about these is quite poor. Although there are a few theoretical attempts to incorporate the finiteness of the potential barrier height between the two materials,[43,44] we prefer to limit our calculations within the model of infinite potential barrier for the surrounding medium without introducing indefinite parameters concerning the potential discontinuity. Another important problem in calculating the exciton-energy spectra is how many electron and hole subbands are to be included in the calculation. This problem is dependent on the quantum-dot size. In the strong confinement regime where the subband energy separations are much larger than the electron-hole Coulomb interaction which is of the order of the exciton binding energy, we may employ the simplest variational wave function composed of only the lowest subband states. As the quantum-dot size is increased, the energy spacings of the quantized subbands become comparable to or smaller than the exciton binding energy. In this regime of the intermediate confinement higher subband states are mixed into even the ground-state exciton wave function. At the same time, the excited states with respect to the electron-hole relative motion are also to be included in the exciton wave functions, especially when the excited excitonic states are concerned. In the weak confinement regime where the quantum-dot size is much larger than the exciton Bohr radius, the quantized subbands are distributed almost continuously and the situation becomes similar to that in the bulk material. The criterion which characterizes the regime of the intermediate confinement is typically written as

$$\min\left[\frac{\hbar^2 D}{2m_e R^2},\frac{\hbar^2 D}{2m_h R^2}\right]\sim\frac{\hbar^2}{2\mu(a_B^*)^2} \tag{2.3}$$

or

$$\frac{R}{a_B^*}\sim\min\left[\left[\frac{D}{1+\sigma}\right]^{1/2},\left[\frac{D\sigma}{1+\sigma}\right]^{1/2}\right]=\left[\frac{D\sigma}{1+\sigma}\right]^{1/2} , \tag{2.4}$$

where $D=(4.49)^2-(3.14)^2$ is the difference between the square of the first zeros of the spherical Bessel functions j_0 and j_1, σ the electron-to-hole mass ratio which is generally smaller than unity, a_B^* the exciton Bohr radius in the bulk material, and μ the electron-hole reduced mass. It is to be noted that the above criterion is derived under the assumption that the wave function vanishes at the crystallite boundary. We can estimate this criterion for typical materials. For GaAs, $\sigma \cong 0.14$ and the above criterion becomes $R/a_B^* \sim 1.12$; for CdS, $\sigma \cong 0.24$ and we have $R/a_B^* \sim 1.41$. Thus the intermediate confinement regime holds for semiconductor microcrystallites having radii of the order of the exciton Bohr radius. In the following, a general scheme will be presented to calculate the exciton-energy spectra in all the confinement regimes.

In calculating the exciton-energy spectra within the model of infinite potential barrier for the surrounding medium, the most suitable basis set for the one-particle wave functions which vanish at the surface of a spherical quantum dot is given as

$$\phi_{lmj}(r,\theta,\varphi)=j_l\left[k_j^l\frac{r}{R}\right]Y_{lm}(\theta,\varphi)\ , \tag{2.5}$$

where j_l is the lth-order spherical Bessel function, k_j^l is its jth zero, and Y_{lm} is one of the spherical harmonics. The exciton wave function can be constructed from a linear combination of products of ϕ_{lmj} for the electron and the hole. At the same time we must take into account the fact that the total angular momentum of an electron-hole pair is a good quantum number because of the spherical symmetry of the Hamiltonian. The angular momenta of the electron, the hole, and the pair will be denoted by l_e, l_h, and $L=l_e+l_h$, respectively. The angular part of the exciton wave function with a total angular momentum L and a magnetic quantum number M can be written as

$$\sum_{m_e}\langle l_e,m_e,l_h,m_h|L,M\rangle Y_{l_e,m_e}(\Omega_e)Y_{l_h,m_h}(\Omega_h)\ , \tag{2.6}$$

using the Clebsch-Gordan coefficient, where Ω denotes the angular variables. As for the radial part wave function, we must include not only the lowest subband state but also the higher subband states and the excited states concerning the electron-hole relative motion. Thus a general exciton wave function can be written as

$$\begin{aligned}\Phi_{LM}(r_e,r_h)=&C_\Phi e^{-\alpha r_{eh}}\\ &\times\sum_n\sum_{l_e,l_h,m_e}\langle l_e,m_e,l_h,m_h|L,M\rangle\\ &\times Y_{l_e,m_e}(\Omega_e)Y_{l_h,m_h}(\Omega_h)\\ &\times r_{eh}^n R_{l_e l_h}^{(n)}(r_e,r_h)\ ,\end{aligned} \tag{2.7}$$

where $r_{eh}=|r_e-r_h|$. The radial part wave function $R_{l_e l_h}^{(n)}$ is a linear combination of products of spherical Bessel functions such as

$$\begin{aligned}R_{l_e l_h}^{(n)}(r_e,r_h)=&\sum_{\bar{l}_e,j_e}\sum_{\bar{l}_h,j_h}C_{l_e l_h}^{(n)}(\bar{l}_e,j_e,\bar{l}_h,j_h)\\ &\times j_{\bar{l}_e}\left[k_{j_e}^{\bar{l}_e}\frac{r_e}{R}\right]j_{\bar{l}_h}\left[k_{j_h}^{\bar{l}_h}\frac{r_h}{R}\right]\ ,\end{aligned} \tag{2.8}$$

where $\bar{l}_e$ and $\bar{l}_h$ are not necessarily identical to l_e and l_h. The parameters in (2.7), namely, α and $\{C_{l_e l_h}^{(n)}\}$, would be determined variationally.

It is easy to see that the optical transition is allowed only to the $L=0$ exciton states. The relevant wave function is given as

$$\begin{aligned}\Phi_{00}(r_e,r_h)=&C_\Phi e^{-\alpha r_{eh}}\sum_n\sum_{l_e,m_e}\langle l_e,m_e,l_e,-m_e|0,0\rangle\\ &\times Y_{l_e,m_e}(\Omega_e)Y_{l_e,-m_e}(\Omega_h)\\ &\times r_{eh}^n R_{l_e l_h}^{(n)}(r_e,r_h)\ .\end{aligned} \tag{2.9}$$

From the property of the Clebsch-Gordan coefficient, i.e, $\langle l,m,l,-m|0,0\rangle=(-1)^{l-m}/\sqrt{2l+1}$, we see that

$$\begin{aligned}\sum_m\langle l,m,l,-m|0,0\rangle Y_{l,m}(\Omega_e)Y_{l,-m}(\Omega_h)&\\ \propto\sum_m Y_{l,m}(\Omega_e)Y_{l,m}^*(\Omega_h)\propto P_l(\cos\Theta_{eh})\ ,&\end{aligned} \tag{2.10}$$

where Θ_{eh} is the angle between the position vectors r_e and r_h. Thus the exciton wave function for $L=0$ can be written as

$$\begin{aligned}\Phi_{00}(r_e,r_h)=C_\Phi e^{-\alpha r_{eh}}\{&R_{00}^{(0)}(r_e,r_h)+r_{eh}R_{00}^{(1)}(r_e,r_h)+r_{eh}^2R_{00}^{(2)}(r_e,r_h)+\cdots\\ &+P_1(\cos\Theta_{eh})[R_{11}^{(0)}(r_e,r_h)+r_{eh}R_{11}^{(1)}(r_e,r_h)+r_{eh}^2R_{11}^{(2)}(r_e,r_h)+\cdots]\\ &+P_2(\cos\Theta_{eh})[R_{22}^{(0)}(r_e,r_h)+r_{eh}R_{22}^{(1)}(r_e,r_h)+r_{eh}^2R_{22}^{(2)}(r_e,r_h)+\cdots]+..\}\ .\end{aligned} \tag{2.11}$$

In the extremely strong confinement regime, we can retain only the lowest-order term in $R_{00}^{(0)}$ and can employ the simplest wave function given as[27]

$$\Phi_{00}(r_e,r_h)=C_\Phi e^{-\alpha r_{eh}}j_0\left[k_1^0\frac{r_e}{R}\right]j_0\left[k_1^0\frac{r_h}{R}\right]\ . \tag{2.12}$$

III. DIELECTRIC CONFINEMENT EFFECT IN THE STRONG CONFINEMENT REGIME

Before going into details of the variational calculation of the exciton energy spectra, we will clarify the salient features of the dielectric confinement effect in the strong confinement regime. As mentioned in Sec. I, the dielectric confinement effect appears more pronounced in the

smaller quantum dot because of the larger opportunity for the electric force lines between an electron and a hole to penetrate through the surrounding medium having a relatively smaller dielectric constant. Thus the exciton-energy spectra in the strong confinement regime are expected to be strongly modified by this dielectric confinement effect. Here the effect on the lowest exciton energy will be examined in detail.

In the extremely strong confinement regime, the envelope function of the lowest-energy exciton state can be given by (2.12). In order to facilitate an analytical treatment, we simplify (2.12) furthermore as

$$\Phi(r_e,r_h)=C_\Phi(1-\alpha r_{eh})j_0\left[k_1^0\frac{r_e}{R}\right]j_0\left[k_1^0\frac{r_h}{R}\right]. \tag{3.1}$$

The spherical coordinates are more convenient than the Hylleraas coordinates[45] for dealing with the surface polarization energy. A key relation in these coordinates is given as

$$\begin{aligned} r_{eh}=\frac{1}{r_{eh}}r_{eh}^2&=\sum_{l=0}^{\infty}\left\{\frac{r_<^l}{r_>^{l+1}}(r_>^2+r_<^2)-2\frac{r_<^l}{r_>^{l-1}}\frac{l}{2l-1}\right.\\ &\left.-2\frac{r_<^{l+2}}{r_>^{l+1}}\frac{l+1}{2l+3}\right\}P_l(\cos\Theta_{eh})\\ &=\sum_{l=0}^{\infty}\mathcal{R}_l(r_e,r_h)P_l(\cos\Theta_{eh}), \end{aligned} \tag{3.2}$$

where $r_>=\max(r_e,r_h)$, $r_<=\min(r_e,r_h)$, and $\mathcal{R}_l(r_e,r_h)$ is introduced for abbreviation. Minimizing the exciton energy with respect to $\bar{\alpha}=\alpha a_B^*$ in the limit of $R\to 0$, we find the optimum value of $\bar{\alpha}$ as

$$\begin{aligned}\bar{\alpha}=-\frac{8}{\pi^5}&\left[4\pi\left(\frac{\pi^4}{16}-I_1I_2\right)+(4I_4-2I_5)\frac{\pi^2}{4}\right.\\ &\left.+I_1(2I_3-\pi^2\alpha_0)\right],\end{aligned} \tag{3.3}$$

with

$$I_1=\int_0^\pi dx_e\int_0^\pi dx_h\sin^2x_e\sin^2x_h\mathcal{R}_0(x_e,x_h), \tag{3.4}$$

$$I_2=\int_0^\pi dx_e\int_0^\pi dx_h\frac{1}{x_>}\sin^2x_e\sin^2x_h, \tag{3.5}$$

$$I_3=\pi\int_0^\pi dx\sin^2x\sum_{n=0}^{\infty}\alpha_n\left[\frac{x}{\pi}\right]^{2n}, \tag{3.6}$$

$$\begin{aligned}I_4=&\int_0^\pi dx_e\int_0^\pi dx_h\sin^2x_e\sin^2x_h\\ &\times\sum_{n=0}^{\infty}\alpha_n\left[\frac{x_ex_h}{\pi^2}\right]^n\frac{\mathcal{R}_n(x_e,x_h)}{2n+1},\end{aligned} \tag{3.7}$$

$$\begin{aligned}I_5=&\int_0^\pi dx_e\int_0^\pi dx_h\sin^2x_e\sin^2x_h\mathcal{R}_0(x_e,x_h)\\ &\times\sum_{n=0}^{\infty}\alpha_n\left[\left[\frac{x_e}{\pi}\right]^{2n}+\left[\frac{x_h}{\pi}\right]^{2n}\right],\end{aligned} \tag{3.8}$$

where $\{\alpha_n\}$ $(n=0,1,2,\ldots)$ are defined by (2.2). The first term within the square brackets of (3.3) corresponds to the result in the absence of the dielectric confinement effect and the second and third terms arise from the surface polarization energy. The lowest exciton energy in effective Rydberg units (Ry*) is calculated as

$$\begin{aligned}E&=\frac{\pi^2}{\bar{R}^2}+\frac{-8\pi I_2+4I_3-2\pi^2\alpha_0}{\pi^2}\frac{1}{\bar{R}}-\bar{\alpha}^2+\mathcal{O}(\bar{R})\\ &=\frac{\pi^2}{\bar{R}^2}+\frac{A_1}{\bar{R}}+A_0+\mathcal{O}(\bar{R}),\end{aligned} \tag{3.9}$$

where $\bar{R}=R/a_B^*$. This is a new formula for the exciton energy in the strong confinement regime which includes the dielectric confinement effect. In the coefficient in front of $1/\bar{R}$, the first term in the numerator comes from the electron-hole direct Coulomb interaction, whereas the second and third terms arise from the surface polarization energy. Of course, when we put $\epsilon_1/\epsilon_2=1$, i.e., $\alpha_n=0$ for all n, the above expressions reproduce the previous results,[38] namely,

$$\bar{\alpha}\cong 0.498,\quad E\cong\frac{\pi^2}{\bar{R}^2}-\frac{3.572}{\bar{R}}-0.248. \tag{3.10}$$

The optimum value of $\bar{\alpha}$ and the coefficients A_0 and A_1 in (3.9) are plotted in Figs. 1 and 2, respectively, as a function of the dielectric-constant ratio ϵ_1/ϵ_2. It is seen that the dielectric confinement has a significant effect on the exciton energy and cannot be treated as a minor perturbation. Previously, when the experimental values of the exciton energy were compared with theoretical calculations, the coefficient A_1 in (3.9) was usually fixed to be -3.572 corresponding to the case without the dielectric confinement effect. However, Fig. 2 shows that the coefficients A_1 and A_0 are sensitively dependent on the dielectric-constant ratio. Especially for the case of a CdS or CdSe microcrystallite embedded in silicate glasses, the dielectric-constant ratio ϵ_1/ϵ_2 is estimated to be about $3\sim 4$ and the dielectric confinement effect would be significant. Thus it would be necessary to reexamine the comparison of the exciton energies between experiments and theories which was done previously.

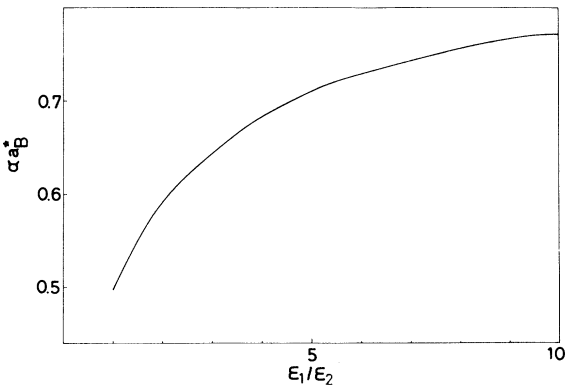

FIG. 1. The variational parameter αa_B^* in the limit of $R\to 0$ is plotted as a function of the dielectric-constant ratio ϵ_1/ϵ_2. In this limit the electron-to-hole mass ratio is irrelevant to the results.

IV. VARIATIONAL CALCULATION OF EXCITON-ENERGY SPECTRA AND THEIR WAVE FUNCTIONS

Now that the functional form of the exciton wave function is fixed, the exciton-energy spectra can be determined by a variational calculation, namely, minimizing the energy given by $\langle\Phi|H|\Phi\rangle/\langle\Phi|\Phi\rangle$. In our case, since the basis functions are not orthogonal to each other, we must solve a generalized eigenvalue problem. Especially, the higher-lying energy spectra have to be determined consecutively by imposing the orthogonality of the wave function on all the previously obtained eigenstates.

In the following we will calculate the energy spectra of the optically allowed exciton states having a zero total angular momentum ($L=0$). The methods of calculation of the normalization integral and various energy components are given in Appendix B. The variational calculation is carried out as follows. First of all, for a fixed value of α, the minimum eigenvalue of a quadratic form with respect to the expansion coefficients $\{C^{(n)}_{l_e l_h}(\bar{l}_e,j_e,\bar{l}_h,j_h)\}$ is determined. Then α is varied in search of a global minimum eigenvalue.

Here we explain the orthogonalization procedure to determine the excited excitonic states successively, although a similar procedure was given concerning the electron subband states in a quantum well under an electric field.[46] Suppose we have determined n excitonic states denoted by $\Phi^{(p)}(r_e,r_h)$ with $p=1,2,\ldots,n$ in the ascending order of the energy and denote by $\Phi(r_e,r_h)$ the wave function of the excited excitonic state to be determined. We must minimize the energy of Φ satisfying the orthogonality of this state to all the lower-lying excitonic states. The orthogonality condition $\langle\Phi^{(p)}|\Phi\rangle=0$ can be reduced to a linear relation with respect to the expansion coefficients $\{C^{(n)}_{l_e l_h}(\bar{l}_e,j_e,\bar{l}_h,j_h)\}$ of Φ which will be abbreviated as $\{c_j\}$. Since $\langle\Phi|\Phi\rangle$ is a quadratic form with respect to $\{c_j\}$, this can be written as

$$\langle\Phi|\Phi\rangle=\sum_{ij} c_i M_{ij}(2\alpha)c_j \ , \tag{4.1}$$

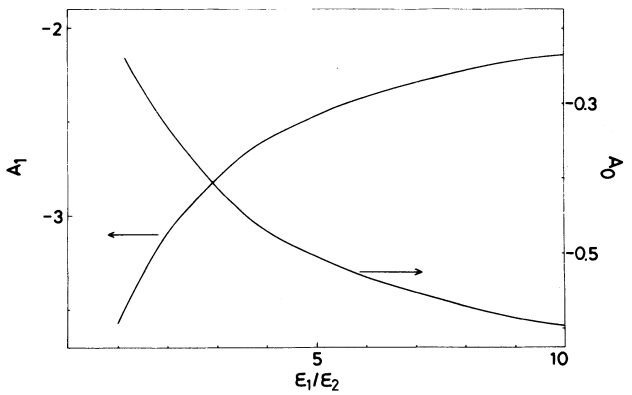

FIG. 2. The coefficients A_0 and A_1 of the lowest exciton energy as given in (3.9) are plotted as a function of the dielectric-constant ratio ϵ_1/ϵ_2. As in Fig. 1, the electron-to-hole mass ratio is irrelevant to the results.

where M_{ij} is a symmetric matrix and the factor 2α comes from the square of $\exp[-\alpha r_{eh}]$ in (2.7). Similarly, the orthogonality condition can be written as

$$\langle\Phi^{(p)}|\Phi\rangle=\sum_{ij} c_i^{(p)} M_{ij}(\alpha+\alpha^{(p)})c_j$$
$$=\sum_j R_j^{(p)} c_j=0 \ , \tag{4.2}$$

where the superscript (p) is attached to the quantities related to the pth eigenstate and $R_j^{(p)}$ is defined by this equation. This series of equations gives the orthogonality conditions for the expansion coefficients $\{c_j\}$. Thus the procedure of energy minimization should be carried out in the restricted space which is orthogonal to n pieces of vectors $\{R^{(p)}\}(p=1,2,\ldots,n)$. In the following, several excitonic states in the lowest-energy region will be calculated. The indices of basis functions in (2.8) employed for a typical calculation are $(\bar{l}_e,\bar{l}_h)=(0,0)$, (1,1), (2,2), (0,1), (1,0), (1,2), (2,1), (0,2), (2,0), and $1\le j_e,j_h\le 3$ and the power n in (2.7) is taken up to 2.

V. EXCITON BINDING ENERGY

The exciton binding energy is known to increase in low-dimensional systems because the spatial overlap between an electron and a hole is increased due to the quantum confinement effect. Following this argument, we can expect that the exciton binding energy is most strongly enhanced in the zero-dimensional system. At the same time, the dielectric confinement effect due to the penetration of the electric force lines into the surrounding medium with a relatively small dielectric constant is also expected to be enhanced in the low-dimensional system, resulting in the enhancement of the exciton binding energy. In this section these features will be examined. First of all, we must note the peculiarity of the zero-dimensional system in defining the exciton binding energy. In the quantum-well system the binding energy of an exciton state associated with a particular pair of conduction and valence subbands is defined in reference to the sum of each subband energy. The sum of subband energies implies the threshold above which the continuum states concerning the electron-hole relative motion are present. Similarly the continuum state has a well-defined meaning in the quantum-wire system since there is at least one spatial dimension along which carriers can move freely. On the other hand, in the quantum-dot system where the carriers are confined in all three dimensions the exciton continuum state associated with a particular pair of electron and hole subbands loses its original meaning. In fact, the electron-hole Coulomb interaction mixes many pairs of electron and hole subbands in forming the excitonic states. The continuum exciton states in a true sense are associated with the subband states which are entirely extended over the surrounding medium. This continuum exciton state does not exist when a model of infinite potential barrier for the surrounding medium is employed as in this paper. Thus the definition of the exciton binding energy in the zero-dimensional system becomes rather indefinite. However, restricting the argument to the lowest-energy exciton, we can define reasonably the exci-

ton binding energy in reference to the sum of energies of the lowest electron and hole subbands, namely,

$$B_X = \langle \phi_{001}(r_e)|H_e|\phi_{001}(r_e)\rangle + \langle \phi_{001}(r_h)|H_h|\phi_{001}(r_h)\rangle - E_{\min} , \quad (5.1)$$

where ϕ_{001} is the lowest-energy subband state defined in (2.5), $E_{\min}$ the lowest exciton energy obtained in Sec. IV, and the single-particle Hamiltonian $H_i (i=e,h)$ contains the kinetic energy and the self-energy part of the surface polarization energy, i.e.,

$$H_i = -\frac{\hbar^2\nabla_i^2}{2m_i} + \frac{e^2}{2R}\sum_{n=0}^{\infty}\alpha_n\left[\frac{r_i}{R}\right]^{2n} . \quad (5.2)$$

Then the exciton binding energy in effective Rydberg units (Ry*) is calculated as

$$B_X = \left[\frac{\pi}{\bar{R}}\right]^2 + \frac{4}{\bar{R}}\sum_{n=0}^{\infty}\frac{\epsilon_1\alpha_n}{\pi^{2n+1}}\int_0^{\pi} dx\, x^{2n}\sin^2 x - E_{\min} , \quad (5.3)$$

where $\bar{R}=R/a_B^*$. This binding energy is proportional to $1/\bar{R}$ in the limit of $R\to 0$ because the kinetic-energy term which is proportional to $1/\bar{R}^2$ is subtracted. As mentioned above, this binding energy does not mean the ionization energy to the true continuum exciton state.

The exciton binding energy is dependent on the quantum-dot size $\bar{R}=R/a_B^*$, the dielectric-constant ratio ϵ_1/ϵ_2, and the electron-to-hole mass ratio m_e/m_h. In Fig. 3, the size dependence of B_X is shown for a fixed value of the electron-to-hole mass ration, i.e., $m_e/m_h=0.2$. The enhancement of the exciton binding energy in the smaller crystallites is due to the increased spatial overlap between an electron and a hole. At the same time, the exciton binding energy increases strongly with an increase in the dielectric-constant ratio ϵ_1/ϵ_2. This is due to the dielectric confinement effect mentioned in Sec. I. This effect can be seen more clearly in Fig. 4 where the exciton binding energy is plotted as a function of the dielectric-constant ratio ϵ_1/ϵ_2. The increasing

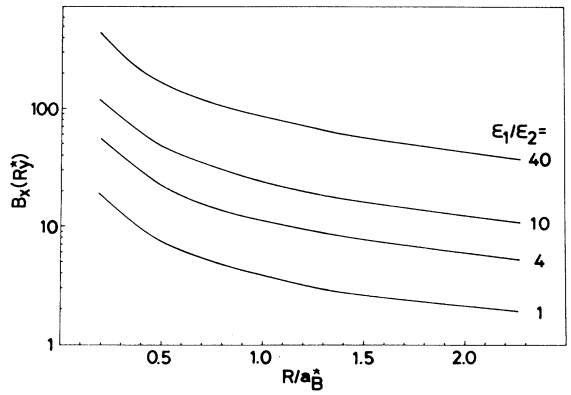

FIG. 3. The binding energy of the lowest exciton state is plotted as a function of the quantum-dot radius for a few values of the dielectric-constant ratio ϵ_1/ϵ_2 with a fixed value of the electron-to-hole mass ratio, i.e., $m_e/m_h=0.2$.

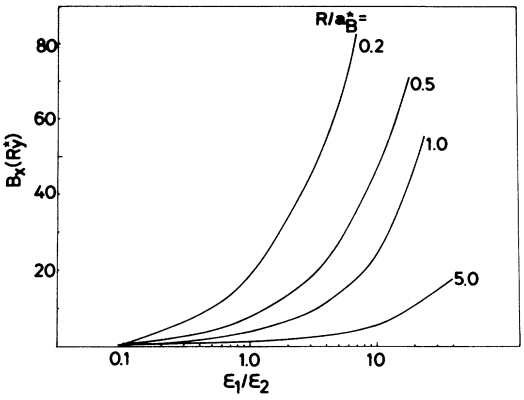

FIG. 4. The binding energy of the lowest exciton state is plotted as a function of the dielectric-constant ratio ϵ_1/ϵ_2 for a few values of the quantum-dot radius with a fixed value of the electron-to-hole mass ratio, i.e., $m_e/m_h=0.2$.

trend is more pronounced for the smaller crystallite. This can be understood as a consequence of the larger opportunity for the electric force lines to penetrate into the surrounding medium in the case of smaller crystallites. The enhancement of the exciton binding energy in the quantum-dot structure becomes more conspicuous when compared with that for the case of a quantum well having a thickness L_z of the same order of magnitude as the quantum-dot diameter.[30] Although a detailed calculation is not yet carried out for the case of a quantum wire, we can expect that the exciton binding energy in the quantum-dot structure is larger than that in the quantum-wire structure whose lateral dimensions are of the same order as the quantum-dot diameter.

In Fig. 5 the optimized values of $\bar{\alpha}=\alpha a_B^*$ in (2.11) are shown as a function of the quantum-dot size for a few values of the dielectric-constant ratio with a fixed value of the electron-to-hole mass ratio, i.e., $m_e/m_h=0.2$. The values of $\bar{\alpha}$ in the limit of $R\to 0$ are 0.498, 0.686, and

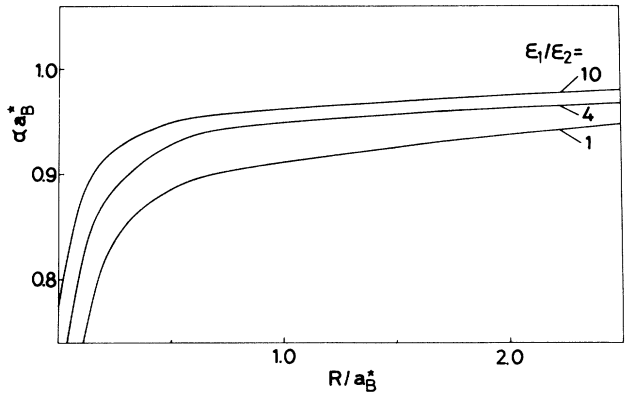

FIG. 5. The optimized value of the variational parameter αa_B^* for the lowest exciton state is plotted as a function of the quantum-dot radius for a few values of the dielectric-constant ratio ϵ_1/ϵ_2 with a fixed value of the electron-to-hole mass ratio, i.e., $m_e/m_h=0.2$.

0.773 for $\epsilon_1/\epsilon_2=1$, 4, and 10, respectively. The decrease of α with decreasing crystallite size implies that the strong quantum confinement weakens the electron-hole Coulomb interaction.

Generally speaking, the electron-hole Coulomb binding becomes stronger for the more asymmetric combination of the electron and hole masses. However, the dependence of B_X on the electron-to-hole mass ratio m_e/m_h is found to be very weak and is not exhibited here. This feature indicates that the admixture of the higher subband states into the lowest-energy exciton state is rather symmetric with respect to the subband indices; namely, the radial components in (2.8) which have a common subband index for the electron and the hole such as $j_l(k_j^l r_e)j_l(k_j^l r_h)$ have a larger amplitude than other components. This trend is preferred in order to increase the electron-hole Coulomb binding due to the increased spatial overlap between the electron and the hole and to lower the exciton energy. Then the subband part of the kinetic energy is determined primarily by the electron-hole reduced mass and is weakly dependent on the electron-to-hole mass ratio since the electron-hole reduced mass is fixed in our calculations. This is a physical origin of the weak dependence of the exciton binding energy on the mass ratio m_e/m_h.

VI. OSCILLATOR STRENGTH OF EXCITONIC TRANSITION

The oscillator strength of the lowest-energy exciton state will be examined concerning its dependence on the quantum-dot size, the dielectric-constant ratio, and the electron-to-hole mass ratio. The magnitude of the oscillator strength is determined by the parameter α and the coefficients of the linear combination of various subband states in (2.8). The optically allowed exciton state is a spin-singlet state given as

$$|\Phi\rangle=\sum_{r_e,r_h}\Phi_{00}(r_e,r_h)\frac{1}{\sqrt{2}}(a^{\dagger}_{cr_e\alpha}a_{vr_h\alpha}+a^{\dagger}_{cr_e\beta}a_{vr_h\beta})|0\rangle\ , \tag{6.1}$$

where the second quantized form in the Wannier representation is employed, $\alpha(\beta)$ in the subscripts indicates the spin-up(down) state, $|0\rangle$ represents the ground state of the system, and Φ_{00} is given by (2.11). Then the matrix element of the momentum operator defined by

$$P=\sum_{r_s}p^0_{cv}(a^{\dagger}_{cr_s\alpha}a_{vr_s\alpha}+a^{\dagger}_{cr_s\beta}a_{vr_s\beta})+\text{H.c.} \tag{6.2}$$

is calculated as

$$\begin{aligned}\langle\Phi|P|0\rangle&=\sqrt{2}p^0_{cv}\sum_{r_s}\Phi_{00}(r_s,r_s)\\&=\sqrt{2}p^0_{cv}C_{\Phi}\sum_{r_s}\{R^{(0)}_{00}(r_s,r_s)+R^{(0)}_{11}(r_s,r_s)\\&\quad+R^{(0)}_{22}(r_s,r_s)+\cdots\}\ ,\end{aligned} \tag{6.3}$$

where p^0_{cv} is the momentum matrix element between the valence-band top and the conduction-band bottom at the Γ point. The oscillator strength of the excitonic transition is defined by

$$f_X=\frac{1}{m_0\hbar\omega_X}|\langle\Phi|P|0\rangle|^2\ , \tag{6.4}$$

and is calculated as

$$f_0|C_{\Phi}\sum_{r_s}\{R^{(0)}_{00}(r_s,r_s)+R^{(0)}_{11}(r_s,r_s)+R^{(0)}_{22}(r_s,r_s)+\cdots\}|^2 \tag{6.5}$$

with

$$f_0=\frac{2}{m_0\hbar\omega_X}|p^0_{cv}|^2\ , \tag{6.6}$$

where m_0 is the free-electron mass. In the following the excitonic transition energy $\hbar\omega_X$ will be assumed to be independent of the crystallite size because the quantum confinement energy is usually much smaller than the original band-gap energy. Then f_0 has a meaning of the oscillator strength of the band-to-band transition at the Γ point. In Fig. 6 the dependence of the normalized oscillator strength f_X/f_0 on the quantum-dot size is shown for a few values of the dielectric-constant ratio ϵ_1/ϵ_2 with a fixed value of the electron-to-hole mass ratio, i.e., $m_e/m_h=0.2$. In the limit of $R\to 0$, the exciton oscillator strength f_X approaches f_0. In fact, this property can be proved exactly as shown in Appendix D. Since f_0 is also the oscillator strength of the atomic transition, it is reasonable that the limit of $R\to 0$ corresponds to the case of a single atom. The magnitude of the oscillator strength is determined by two factors concerning the electron-hole relative motion and the exciton center-of-mass motion. The former is related to the parameter α in (6.1), whereas the latter comes from the summation over r_s in (6.5) and is roughly proportional to the number of unit cells contained in a quantum dot. As a result the exciton oscillator strength increases with increasing crystal-

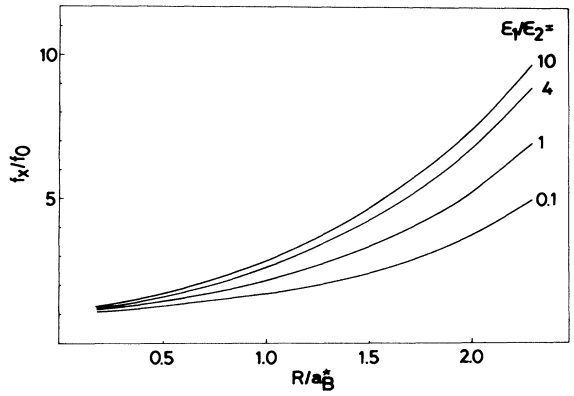

FIG. 6. The normalized oscillator strength f_X/f_0 for the lowest exciton state is plotted as a function of the quantum-dot radius for a few values of the dielectric-constant ratio ϵ_1/ϵ_2 with a fixed value of the electron-to-hole mass ratio, i.e., $m_e/m_h=0.2$.

lite size. This increasing trend is stronger for a larger value of the dielectric-constant ratio. This is a consequence of the increased electron-hole Coulomb binding due to the dielectric confinement effect. In order to see this dielectric confinement effect more clearly, we plot the exciton oscillator strength in Fig. 7 as a function of the dielectric-constant ratio for several values of the quantum-dot size with a fixed value of m_e/m_h ($=0.2$). The enhancement factor of the oscillator strength is larger than that for the case of a quantum well having a thickness of the same magnitude as the quantum-dot diameter.[30] Thus we can confirm that the dielectric confinement effect appears stronger in the lower-dimensional structures.

On the other hand, the dependence of the oscillator strength on the electron-to-hole mass ratio is exhibited in Fig. 8 for several values of the quantum-dot radius with a fixed value of the dielectric-constant ratio, i.e., $\epsilon_1/\epsilon_2=4.0$. This dependence is rather weak reflecting the insensitivity of the envelope function to the mass ratio as noted in Sec. V. However, for the case of $R/a_B^*=3$, the dependence is not negligible. When the hole is heavier than the electron, the energy spacings of the hole subbands are smaller than those of the electron subbands. Furthermore, the subband mixing occurs strongly in a larger crystallite. Under this situation the off-diagonal transitions in which the quantum numbers (l,j) of the electron and hole subbands in (2.8) are different are easily mixed into the ground excitonic state. This admixture decreases the exciton oscillator strength. The decrease of the exciton oscillator strength with decreasing electron-to-hole mass ratio can be interpreted in this way for the case of $R/a_B^*=3$.

VII. SUBBAND MIXING DUE TO COULOMB INTERACTION

If the Coulomb interaction between an electron and a hole is neglected, the interband transition is allowed only for a pair of electron and hole subbands having the same

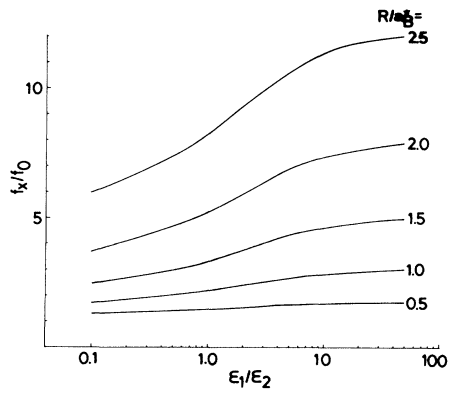

FIG. 7. The normalized oscillator strength f_X/f_0 for the lowest exciton state is plotted as a function of the dielectric-constant ratio ϵ_1/ϵ_2 for several values of the quantum-dot radius with a fixed value of the electron-to-hole mass ratio, i.e., $m_e/m_h=0.2$.

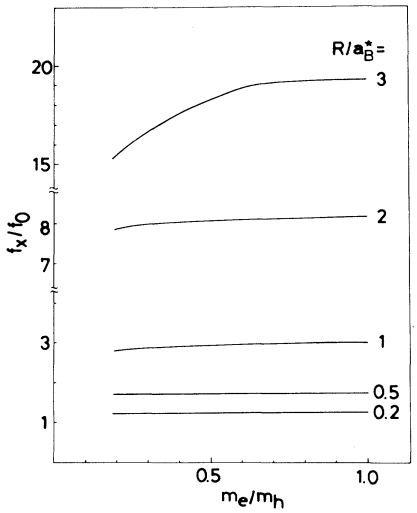

FIG. 8. The normalized oscillator strength f_X/f_0 for the lowest exciton state is plotted as a function of the electron-to-hole mass ratio m_e/m_h for several values of the quantum-dot radius with a fixed value of the dielectric-constant ratio, i.e., $\epsilon_1/\epsilon_2=4$.

angular momentum l and the same radial quantum number j defined in (2.8), because of the orthogonality of the envelope functions for different numbers of (l,j). In the presence of the Coulomb interaction, the subband mixing occurs and the interband transitions between electron and hole subbands having different numbers of (l,j) become allowed. In order to see this subband mixing clearly, we show in Figs. 9(a) and 9(b) the lowest part of the exciton-energy spectra for $R/a_B^*=1$ and 3, respectively, with fixed values of ϵ_1/ϵ_2 ($=4.0$) and m_e/m_h ($=0.2$). The oscillator strength of each transition is represented by the height of the line spectrum. The energy position of the interband transition between an electron subband (l,j) and a hole subband (l',j') in the absence of the Coulomb interaction is depicted by a vertical bar in the figure where the upper (lower) pair of numbers denote the subband indices of the electron (hole). Hereafter this transition will be denoted as $(l,j)\rightarrow(l',j')$. The lowest excitonic transition is mainly composed of the $(0,1)\rightarrow(0,1)$ transition, although its energy position is lowered by the exciton binding energy. The next lowest excitonic level is considered to be composed of combination of transitions such as $(0,1)\rightarrow(1,1)$, $(0,1)\rightarrow(0,2)$, $(0,1)\rightarrow(2,1)$, and so on. In a similar way, the third excitonic level in Fig. 9(a) and the fourth excitonic level in Fig. 9(b) can be considered to be composed mainly of the $(1,1)\rightarrow(1,1)$ transition.

Now we will focus our attention on the second excitonic level. This level represents an off-diagonal transition in which the quantum numbers of the electron and hole subbands are different and which is optically forbidden in the absence of the Coulomb interaction. Thus the oscillator strength of this transition gives a measure of strength of the subband mixing due to the Coulomb interaction. From this viewpoint, the subband mixing is considered to be stronger for $R/a_B^*=3$ than for $R/a_B^*=1$, because the

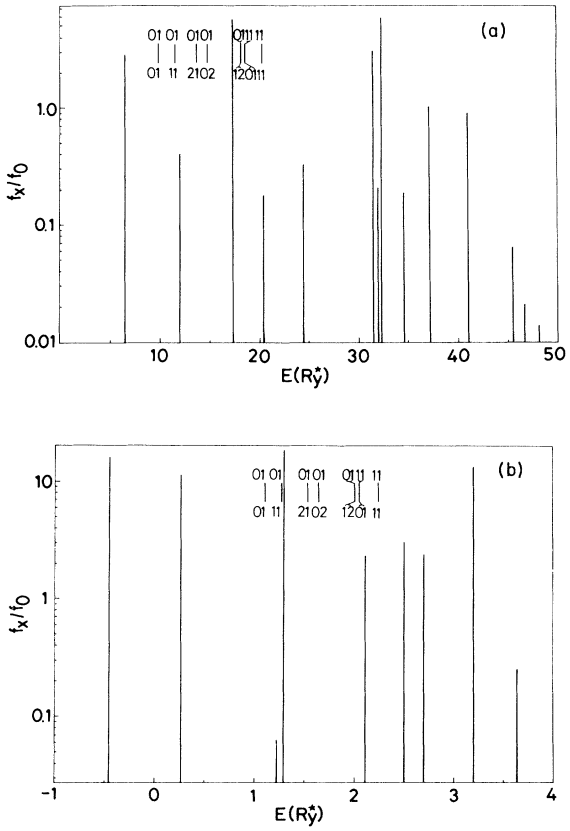

FIG. 9. Exciton energy spectra in a quantum dot are plotted in the lowest-energy part for the radius (a) $R/a_B^*=1$ and (b) $R/a_B^*=3$, with common parameters, i.e., $\epsilon_1/\epsilon_2=4$ and $m_e/m_h=0.2$. A vertical bar indicates the energy position of an interband transition between the electron subband (l,j) (upper indices) and the hole subband (l',j') (lower indices) in the absence of the Coulomb interaction.

ratio of the oscillator strength of the second excitonic level to that of the lowest one is larger in the former case.

VIII. ELECTRON-HOLE EXCHANGE INTERACTION IN QUANTUM-DOT STRUCTURES

It is well known that in the bulk material the electron-hole exchange interaction contains a short-range (analytical) part and a long-range (nonanalytical) part, and that the latter part gives rise to the longitudinal-transverse exciton splitting. Both components are proportional to the probability of the spatial overlap between an electron and a hole. In a low-dimensional system the quantum confinement effect generally increases the electron-hole spatial overlap and consequently enhances the electron-hole exchange interaction. In fact, the enhancement of the electron-hole exchange interaction in the two-dimensional quantum-well structure has been studied both experimentally[47,48] and theoretically.[49–51] As an extension of this argument, the electron-hole exchange interaction is expected to be enhanced more strongly in the quantum-dot structure. However, the long-range part of the exchange interaction is considered to show a different behavior from that of the bulk material because the concept of wave vector associated with the center-of-mass motion of the exciton is completely missing due to the three-dimensional confinement. Here we will examine the dependence of the short-range part of the exchange interaction on the quantum-dot size and on the dielectric-constant ratio between the quantum dot and the surrounding medium. Furthermore we will clarify a peculiar feature of the long-range part of the exchange interaction.

The expression of the electron-hole exchange interaction in the site representation is derived in Appendix E. Taking into account the localized nature of the Wannier orbitals, we can assume $r_e=r_h$ and $r_e'=r_h'$ in (E5) of the electron-hole exchange term and approximate as

$$\delta_{\sigma,\tau}\delta_{\sigma',\tau'}\delta_{r_e,r_h}\delta_{r_e',r_h'}V(\nu\tau r_e,\mu'\sigma' r_h';\nu'\tau r_e',\mu\sigma r_h)\ . \tag{8.1}$$

When we consider only a single band for both the conduction ($\nu=\nu'=c$) and valence ($\mu=\mu'=v$) bands, the exchange energy is given by

$$2\sum_{r_e,r_e'}\Phi^*(r_e,r_e)\Phi(r_e',r_e')V(cr_e,vr_e';cr_e',vr_e) \tag{8.2}$$

for a spin-singlet exciton state. Here the spin indices in the matrix element of V are dropped. Of course, the exchange energy vanishes for a spin-triplet exciton state and this gives rise to the singlet-triplet energy splitting. Then, following the usual procedure,[33] we can separate the short- and long-range parts of the exchange energy as

$$2\sum_{r_e,r_e'}{}'\Phi^*(r_e,r_e)\Phi(r_e',r_e')V(cr_e,vr_e';cr_e',vr_e)$$
$$+2\sum_{r_e\neq r_e'}\Phi^*(r_e,r_e)\Phi(r_e',r_e')^t\mu_{cv}\frac{1-3n\cdot{}^tn}{|r_e-r_e'|^3}\mu_{vc}\ , \tag{8.3}$$

with $\mu_{cv}=e\int d^3r\,\phi^*_{cr_e}(r)(\mathbf{r}-\mathbf{r}_e)\phi_{vr_e}(r)$ and $n=(\mathbf{r}_e-\mathbf{r}_e')/|\mathbf{r}_e-\mathbf{r}_e'|$, where $n\cdot{}^tn$ is a dyadic form and the sum over r_e' in the first term is taken over a region around r_e with a dimension of the order of the lattice constant and the sum in the second term is taken over the complementary region. It should be noted that this kind of separation is valid only for large crystallites. In a very small crystallite containing as few as, e.g., a few tens of atoms, we would have to calculate (8.2) directly.

In the calculation of the short-range exchange energy we can put $r_e=r_e'$ in the first term of (8.3) and obtain

$$2N_c\sum_{r_e}|\Phi(r_e,r_e)|^2V(cr_e,vr_e;cr_e,vr_e)$$
$$\cong 2N_cV(cr_0,vr_0;cr_0,vr_0)\sum_{r_e}|\Phi(r_e,r_e)|^2\ , \tag{8.4}$$

where N_c is the number of unit cells contained in the relevant region of the sum which is usually taken to be 1, the matrix element of V is put in front of the summation because of the translational invariance of V, and r_0 is an arbitrary lattice point. In order to see the enhancement

of the short-range exchange energy in a quantum dot, it is appropriate to compare it with the corresponding expression for the bulk material. In the latter case, the envelope function can be taken as

$$\Phi(r_e,r_h)=\left[\frac{v_0}{N}\right]^{1/2} e^{iKR}\frac{e^{-|r_e-r_h|/a_B^*}}{[\pi(a_B^*)^3]^{1/2}}\ , \tag{8.5}$$

where v_0 is the volume of a unit cell, Nv_0 the quantization volume, R the exciton center-of-mass coordinate, and K the associated wave-vector. The exchange energy is calculated as[52]

$$\frac{2v_0}{\pi(a_B^*)^3}V(cr_0,vr_0;cr_0,vr_0) - \frac{8}{3\epsilon_1(a_B^*)^3}{}^t\mu_{cv}(1-3\hat{\mathbf{K}}\cdot{}^t\hat{\mathbf{K}})\mu_{vc}\ , \tag{8.6}$$

where the first term is the short-range exchange energy, the second term the long-range exchange energy arising from the dipole-dipole interaction, ϵ_1 the dielectric constant of the semiconductor material, and $\hat{\mathbf{K}}$ a unit vector in the direction of K. Then the enhancement factor of the short-range exchange energy in a quantum dot over the bulk value can be estimated by

$$\beta_{\text{exch}}\equiv\frac{\pi(a_B^*)^3}{v_0}\sum_{r_s}|\Phi(r_s,r_s)|^2\ . \tag{8.7}$$

It is interesting to note that this factor is different from the enhancement factor for the exciton oscillator strength in (6.5) which is proportional to $|\sum_{r_s}\Phi(r_s,r_s)|^2$. As a consequence, the oscillator strength and the short-range exchange energy show different behaviors as a function of the quantum-dot size. In Fig. 10 the enhancement factor in (8.7) is plotted as a function of the quantum-dot size for a few values of the dielectric-constant ratio ϵ_1/ϵ_2 with a fixed value of m_e/m_h ($=0.2$). The exchange energy increases as the crystallite size is decreased in a striking contrast to the exciton oscillator strength. The enhancement factor of the exchange energy in the limit of $R\to 0$ is inversely proportional to R^3 as shown in Appendix D. This theoretical behavior is shown by a dashed line in the figure. This enhancement factor cannot become indefinitely large because the quantum-dot size cannot be reduced smaller than a unit cell. The attainable minimum value of $(R/a_B^*)^3$ is of the order of $v_0/(a_B^*)^3$. Furthermore the finiteness of the potential barrier of the surrounding medium leads to incomplete confinement of carriers and reduces the spatial overlap between an electron and a hole. Thus the enhancement factor becomes saturated at a certain level as the quantum-dot size is reduced. On the other hand, as the crystallite size is increased, the situation becomes similar to that in the bulk material and the enhancement factor approaches unity.

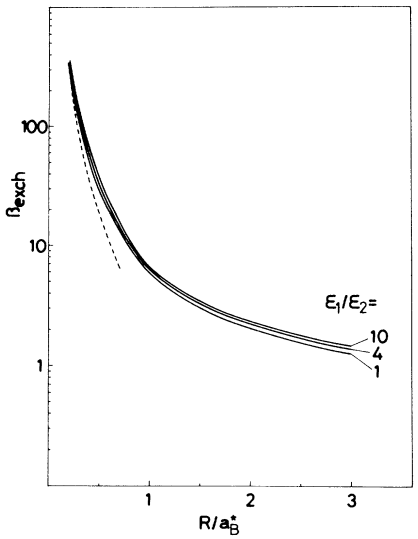

FIG. 10. The enhancement factor of the short-range part of the electron-hole exchange energy is plotted as a function of the quantum-dot radius for a few values of the dielectric-constant ratio ϵ_1/ϵ_2 with a fixed value of the electron-to-hole mass ratio, i.e., $m_e/m_h=0.2$. The dashed line is a theoretical curve in the limit of strong quantum confinement.

We remark briefly that the exchange energy increases with increasing dielectric-constant ratio due to the dielectric confinement effect but the dependence is rather weak.

From the above consideration, it is found that the short-range exchange energy in a quantum dot can be enhanced very much over the bulk value in materials having a large exciton Bohr radius, e.g., GaAs. On the other hand, in materials whose exciton Bohr radius is rather small, e.g., CuCl, the exchange energy cannot be enhanced very much over the bulk value even in a smallest quantum dot.

Now we will discuss the long-range part of the electron-hole exchange energy, namely, the second term of (8.3). In the calculation of this term the integration over r_e' is carried out excluding a small region around r_e. This prescription will be denoted by a superscript c on the integral sign. Noting the relation

$$\frac{3n_\alpha n_\beta-\delta_{\alpha\beta}}{|r-r'|^3}=\frac{\partial^2}{\partial r_\alpha\partial r_\beta}\left[\frac{1}{|r-r'|}\right]\ , \tag{8.8}$$

where α and β are the Cartesian components, we can rewrite the second term of (8.3) as

$$\frac{-2}{v_0^2}\int d^3r\int^c d^3r'\Phi^*(r,r)\mu_{cv}\cdot\nabla_r\nabla_r\cdot\left[\frac{\mu_{vc}}{|r-r'|}\Phi(r',r')\right]\ , \tag{8.9}$$

where the subscript e on the coordinates is omitted. Then making use of the relation

$$\nabla_r\nabla_r\cdot\int^c d^3r'\frac{Q(r')}{|r-r'|}=\int^c d^3r'\nabla_r\nabla_r\cdot\left[\frac{Q(r')}{|r-r'|}\right]-\frac{4\pi}{3}Q(r)\ , \tag{8.10}$$

where $Q(r)$ is an arbitrary vector field, we can rewrite (8.9) as

$$\frac{-2}{v_0^2}\int d^3r\,\Phi^*(r,r)\mu_{cv}\cdot\left[\frac{4\pi}{3}\mu_{vc}\Phi(r,r)+\nabla_r\nabla_r\cdot\int^c d^3r'\frac{\mu_{vc}}{|r-r'|}\Phi(r',r')\right] . \tag{8.11}$$

This expression is quite general and is applicable to any shape of the quantum dot. When the envelope function in a spherical quantum dot is expanded as

$$\Phi(r',r')=\sum_{l,m}\Phi_{lm}(r')Y_{lm}(\Omega') , \tag{8.12}$$

we have

$$\int^c d^3r'\frac{\mu_{vc}}{|r-r'|}\Phi(r',r')=4\pi\mu_{vc}\sum_{l,m}\frac{Y_{lm}(\Omega)F_{lm}(r)}{2l+1} , \tag{8.13}$$

with

$$F_{lm}(r)=\frac{1}{r^{l+1}}\int_0^r dr'(r')^{l+2}\Phi_{lm}(r')+r^l\int_r^R dr'\frac{\Phi_{lm}(r')}{(r')^{l-1}} . \tag{8.14}$$

Then (8.11) can be decomposed as

$$\frac{-8\pi}{v_0^2}\int d^3r\left[\tfrac{1}{3}\mu_{cv}\cdot\mu_{vc}|\Phi(r,r)|^2+\Phi^*(r,r)\sum_{l,m}\frac{1}{2l+1}\left\{\mu_{cv}\cdot\nabla(\mu_{vc}\cdot\nabla Y_{lm})F_{lm}(r)\right.\right.$$
$$+\left[2(\mu_{cv}\cdot a_r)(\mu_{vc}\cdot\nabla Y_{lm})+\frac{\mu_{cv}\cdot\mu_{vc}}{r}Y_{lm}\right]\frac{dF_{lm}}{dr}$$
$$\left.\left.+(\mu_{cv}\cdot a_r)(\mu_{vc}\cdot a_r)\left[\frac{d^2F_{lm}}{dr^2}-\frac{1}{r}\frac{dF_{lm}}{dr}\right]Y_{lm}\right\}\right] , \tag{8.15}$$

where a_r is a unit vector in the radial direction. For the optically allowed exciton state as given in (2.11), $\Phi(r',r')$ in (8.12) contains only an s-like component with $l=m=0$ and (8.15) is proportional to an integral given by

$$^t\mu_{cv}\int d\Omega(3a_r\cdot{}^t a_r-1)\mu_{vc} , \tag{8.16}$$

which vanishes identically.

Consequently the long-range part of the exchange energy vanishes for the optically allowed exciton state in a spherical quantum dot. However, if the shape of the quantum dot deviates from the sphere, the envelope function in (8.12) has various components of spherical harmonics and (8.15) would not vanish in general. Thus the long-range part of the exchange energy is sensitively dependent on the shape of the quantum dot. At the same time, it should be noted that the valence-band degeneracy changes the symmetry of the envelope function and the long-range part of the exchange energy would remain finite even in a spherical quantum dot.

The relevant quantities in estimating the absolute values of the exchange energies are $V(cr_0,vr_0;cr_0,vr_0)$ and $|\mu_{cv}|^2$. These can be estimated from the energy positions of the longitudinal, transverse, and spin-triplet exciton states in the bulk materials. When we introduce the quantities

$$\Delta_{\rm ex}=\frac{2v_0}{\pi(a_B^*)^3}V(cr_0,vr_0;cr_0,vr_0) , \tag{8.17}$$

$$\Delta_{\rm dip}=\frac{8}{3}\frac{|\mu_{cv}|^2}{\epsilon_1(a_B^*)^3} , \tag{8.18}$$

$\Delta_{\rm dip}$ is given by one-third of the longitudinal-transverse splitting energy Δ_{LT} and $\Delta_{\rm ex}$ can be determined from the singlet-triplet splitting energy Δ_{ST}. For CuCl, $\Delta_{\rm dip}$ and $\Delta_{\rm ex}$ are estimated as 1.8 and 10.5 meV, respectively.[53] On the basis of the above arguments, we can expect that the short-range exchange energy $\Delta_{\rm ex}$ in a CuCl crystallite would not be enhanced and would be of the order of 10 meV, since the exciton Bohr radius in CuCl is of the same order as the lattice constant. For GaAs, although $\Delta_{\rm ex}$ is not known precisely, we can deduce that $\Delta_{\rm ex}$ is about two orders of magnitude smaller than that of CuCl because the measured values of $\Delta_{\rm LT}$ (Refs. 54 and 55) and $\Delta_{\rm ST}$ (Ref. 55) are about two orders of magnitude smaller than those of CuCl. The enhancement factor of the short-range exchange energy in a quantum dot is proportional to $(a_B^*)^3/R^3$ and is estimated to be about 300 for $R\cong 20$ Å. Thus for a GaAs quantum dot with radius about 20 Å, the short-range exchange energy is expected to be of the order of 10 meV. Although these exchange energies are not very large compared with the quantum confinement energy, the excitonic level structure would show various interesting features reflecting the interplay among the subband quantization, the electron-hole exchange interaction, the valence-band degeneracy, the spin-orbit interaction, and possibly the magnetic-field-induced subband mixing. This problem is very interesting but is left for future study.

IX. SUMMARY AND DISCUSSION

A general scheme was established within the effective-mass approximation to calculate systematically the exci-

tonic energy spectra in a semiconductor quantum dot including the dielectric confinement effect. This effect was shown to appear most pronounced in the quantum-dot structure in comparison with the quantum-well and quantum-wire structures. We clarified the significance of the dielectric confinement effect on the exciton energy in the strong confinement regime and pointed out the necessity of reexamination of the previous comparison of the exciton energies between experiments and theories. We investigated the dependence of the binding energy and the oscillator strength of the lowest-energy excitonic state on the quantum-dot radius, the electron-to-hole mass ratio, and the dielectric-constant ratio between the quantum dot and the surrounding medium. The subband mixing effect due to the electron-hole Coulomb interaction was shown unambiguously in the calculated exciton energy spectra by looking at the dependence on the quantum-dot size of the intensity ratio of the second lowest excitonic transition to the lowest one. The electron-hole exchange interaction in a quantum dot was discussed for the first time. The short-range part of the exchange energy was shown to increase in proportion to the inverse of the volume of the quantum dot as the quantum-dot size is reduced. On the other hand, the long-range part of the exchange energy was found to be sensitively dependent on the shape of the quantum dot. Especially, it vanishes for the optically allowed excitonic states in a spherical quantum dot.

One of the most important problems concerning the subband mixing discussed in Sec. VII is the exciton–LO-phonon interaction. As noted before,[56,57] if the lowest-energy exciton state is composed of a pair of the lowest subband states of an electron and a hole, the Fröhlich coupling between the exciton and the LO phonon vanishes because this coupling is proportional to an integral of the phonon mode function multiplied by the total charge density of the electron and the hole. The same situation holds even if the excitonic state is composed of various combinations of subband pairs as far as the subband index (l,j) in (2.8) is the same for the electron and the hole. Thus in order to estimate the strength of the exciton–LO-phonon coupling, we must know precisely the coefficients of linear combination in (2.8). The exciton–LO-phonon interaction in a quantum dot will be discussed in detail elsewhere in conjunction with the exciton relaxation processes.

Finally we will mention briefly the possibility of experimental observation of the dielectric confinement effect. In order to change systematically the dielectric-constant ratio between the quantum-dot material and the surrounding medium, it would be favorable to use colloidal suspensions of microcrystallites because the dielectric-constant ratio can be varied by changing the solvent. The exciton binding energy is not easy to measure directly from the absorption spectra since it is rather difficult to identify definitely the position of the subband energy gap. Furthermore the absorption spectrum is inhomogeneously broadened due to the size distribution of microcrystallites. A relevant means to estimate the exciton binding energy is to measure the photoluminescence intensity as a function of the inverse temperature. We can confirm the dielectric confinement effect from the dependence of the activation energy on the dielectric-constant ratio.

ACKNOWLEDGMENTS

The author would like to thank Dr. N. Uesugi and Dr. Y. Horikoshi for continual encouragement.

APPENDIX A: DIELECTRIC CONFINEMENT POTENTIAL IN A CUBOIDAL QUANTUM DOT

In this appendix the Coulomb interaction between an electron and a hole in low-dimensional structures will be summarized. The dielectric confinement effect can be incorporated most conveniently in terms of the image charges induced by the difference in the dielectric constant between the semiconductor material and the surrounding medium.

1. Quantum well

The x axis is chosen in the direction perpendicular to the well layers and the well thickness is $2a$. The dielectric confinement potential for an electron-hole pair within the quantum well is calculated as[30]

$$-\frac{e^2}{\epsilon_1}\sum_{n=-\infty}^{\infty}\frac{\xi^{|n|}}{[(x_e-x_{hn})^2+(y_e-y_h)^2+(z_e-z_h)^2]^{1/2}}+\frac{e^2}{2\epsilon_1}\sum_{n=-\infty}^{\infty}{}'\frac{\xi^{|n|}}{|x_e-x_{en}|}+\frac{e^2}{2\epsilon_1}\sum_{n=-\infty}^{\infty}{}'\frac{\xi^{|n|}}{|x_h-x_{hn}|}\ , \tag{A1}$$

with

$$x_{\alpha n}=2na+(-1)^n x_\alpha \quad (\alpha=e \text{ or } h;\ \ n=-\infty,\ldots,\infty) \tag{A2}$$

$$\xi=\frac{\epsilon_1-\epsilon_2}{\epsilon_1+\epsilon_2}\ , \tag{A3}$$

where the subscript e (h) is attached to the quantities related to the electron (hole), ϵ_1 (ϵ_2) is the dielectric constant of the quantum-well (barrier) material, and the prime indicates the exclusion of the $n=0$ term in the summation.

2. Rectangular quantum wire

The axis of the quantum wire is chosen in the z direction and the lateral dimensions in the x and y directions are denoted by $2a$ and $2b$. The dielectric confinement potential for an electron-hole pair within the quantum wire is calculated as

$$-\frac{e^2}{\epsilon_1}\sum_{l=-\infty}^{\infty}\sum_{m=-\infty}^{\infty}\frac{\xi^{|l|+|m|}}{[(x_e-x_{hlm})^2+(y_e-y_{hlm})^2+(z_e-z_h)^2]^{1/2}}$$
$$+\frac{e^2}{2\epsilon_1}\sum_{l=-\infty}^{\infty}\sum_{m=-\infty}^{\infty}{}'\frac{\xi^{|l|+|m|}}{[(x_e-x_{elm})^2+(y_e-y_{elm})^2]^{1/2}}+\frac{e^2}{2\epsilon_1}\sum_{l=-\infty}^{\infty}\sum_{m=-\infty}^{\infty}{}'\frac{\xi^{|l|+|m|}}{[(x_h-x_{hlm})^2+(y_h-y_{hlm})^2]^{1/2}} \tag{A4}$$

with

$$(x_{\alpha lm},y_{\alpha lm},z_\alpha)=[2la+(-1)^l x_\alpha,2mb+(-1)^m y_\alpha,z_\alpha]\quad(\alpha=e\text{ or }h;\quad l,m=-\infty,\ldots,\infty)\,, \tag{A5}$$

where the prime indicates the exclusion of the $l=m=0$ term in the summation.

3. Cuboidal quantum dot

We consider a cuboid having the dimension of $2a$, $2b$, and $2c$ in the x, y, and z directions, respectively. The dielectric confinement potential for an electron-hole pair within the cuboidal quantum dot is calculated as

$$-\frac{e^2}{\epsilon_1}\sum_{l=-\infty}^{\infty}\sum_{m=-\infty}^{\infty}\sum_{n=-\infty}^{\infty}\frac{\xi^{|l|+|m|+|n|}}{[(x_e-x_{hlmn})^2+(y_e-y_{hlmn})^2+(z_e-z_{hlmn})^2]^{1/2}}$$
$$+\frac{e^2}{2\epsilon_1}\sum_{l=-\infty}^{\infty}\sum_{m=-\infty}^{\infty}\sum_{n=-\infty}^{\infty}{}'\frac{\xi^{|l|+|m|+|n|}}{[(x_e-x_{elmn})^2+(y_e-y_{elmn})^2+(z_e-z_{elmn})^2]^{1/2}}$$
$$+\frac{e^2}{2\epsilon_1}\sum_{l=-\infty}^{\infty}\sum_{m=-\infty}^{\infty}\sum_{n=-\infty}^{\infty}{}'\frac{\xi^{|l|+|m|+|n|}}{[(x_h-x_{hlmn})^2+(y_h-y_{hlmn})^2+(z_h-z_{hlmn})^2]^{1/2}} \tag{A6}$$

with

$$(x_{\alpha lmn},y_{\alpha lmn},z_{\alpha lmn})=[2la+(-1)^l x_\alpha,2mb+(-1)^m y_\alpha,2nc+(-1)^n z_\alpha]\quad(\alpha=e\text{ or }h;l,m,n=-\infty,\ldots,\infty)\,, \tag{A7}$$

where the prime indicates the exclusion of the $l=m=n=0$ term in the summation.

APPENDIX B: CALCULATION OF THE NORMALIZATION INTEGRAL AND VARIOUS ENERGY COMPONENTS

Here we explain briefly the methods of calculation of the normalization integral and the various energy components associated with the $L=0$ exciton wave functions given in (2.11).

1. Calculation of normalization integral, Coulomb energy, and surface polarization energy

A typical integral appearing in the normalization integral, Coulomb energy, and surface polarization energy has a form given as

$$\int d^3r_e\int d^3r_h\, e^{-2\alpha r_{eh}} r_{eh}^n P_l(\cos\Theta_{eh})\, r_e^p r_h^q \times j_{l_1}\left[k_{i_1}^{l_1}\frac{r_e}{R}\right] j_{l_2}\left[k_{i_2}^{l_2}\frac{r_e}{R}\right] j_{l_3}\left[k_{i_3}^{l_3}\frac{r_h}{R}\right] \times j_{l_4}\left[k_{i_4}^{l_4}\frac{r_h}{R}\right], \tag{B1}$$

where l, n, p, q, and $(l_j,i_j,j=1\sim4)$ are integer numbers. Introducing the Fourier transform such that

$$r_{eh}^n e^{-\alpha r_{eh}}=\int d^3k\, g^{(n)}(k,\alpha)e^{ik(r_e-r_h)} \tag{B2}$$

and substituting the expansion of a plane wave in terms of the spherical harmonics, we obtain

$$r_{eh}^n e^{-\alpha r_{eh}}=(4\pi)^2\int_0^\infty dk\, k^2 g^{(n)}(k,\alpha)\times\sum_{l=0}^{\infty} j_l(kr_e)j_l(kr_h)\times\sum_{m=-l}^{l} Y_{lm}^*(\Omega_e)Y_{lm}(\Omega_h)$$
$$=4\pi\sum_{l=0}^{\infty}(2l+1)G_l^{(n)}(r_e,r_h,\alpha)P_l(\cos\Theta_{eh}), \tag{B3}$$

with

$$G_l^{(n)}(r_e,r_h,\alpha)=\int_0^\infty dk\, k^2 g^{(n)}(k,\alpha)j_l(kr_e)j_l(kr_h)\,. \tag{B4}$$

The explicit expression of $G_l^{(n)}(r_e,r_h,\alpha)$ is given in Appendix C. Then carrying out the integration over the angular variables in (B1), we are left with a radial integral given as

$$\int_0^R dr_e r_e^{p+2}\int_0^R dr_h r_h^{q+2}G_l^{(n)}(r_e,r_h,2\alpha)\times j_{l_1}\left[k_{i_1}^{l_1}\frac{r_e}{R}\right] j_{l_2}\left[k_{i_2}^{l_2}\frac{r_e}{R}\right] j_{l_3}\left[k_{i_3}^{l_3}\frac{r_h}{R}\right] j_{l_4}\left[k_{i_4}^{l_4}\frac{r_h}{R}\right]. \tag{B5}$$

This type of integral can be calculated numerically.

2. Calculation of the kinetic energy

In order to reduce the expression of the kinetic energy to a tractable form, we make full use of the boundary

condition that the envelope function vanishes at the quantum-dot surface. In the following, the calculation of only the electronic part of the kinetic energy will be explained because the hole part can be calculated in exactly the same way. Applying the Gauss formula and noticing the reality of the envelope function, we have

$$-\int d\tau \Phi \nabla_e^2 \Phi = \int d\tau (\nabla_e \Phi)^2 , \tag{B6}$$

where $d\tau = d^3 r_e d^3 r_h$ and ∇_e is the gradient operator with respect to the electron coordinate. The exciton envelope function can be generally written as

$$\Phi(r_e, r_h) = \sum_i c_i g_i(r_e, r_h) R_i(|r_e|, |r_h|) , \tag{B7}$$

where g_i contains the factors such as r_{eh}^n, $e^{-\alpha r_{eh}}$, and $P_n(\cos\Theta_{eh})$ and R_i includes only the radial coordinates like the function of (2.8). The essential part of the calculation can be explained by considering a typical term appearing in (B6) which is given as

$$\int d\tau [(\nabla_e g_1) R_1 + g_1 (\nabla_e R_1)][(\nabla_e g_2) R_2 + g_2 (\nabla_e R_2)] . \tag{B8}$$

Applying the Gauss formula, we have

$$\begin{aligned} \int d\tau \{ &(\nabla_e g_1)(\nabla_e g_2) R_1 R_2 \\ &- \tfrac{1}{2} g_1 g_2 [(\nabla_e^2 R_1) R_2 + R_1 (\nabla_e^2 R_2)] \\ &+ \tfrac{1}{2} [(\nabla_e g_1) g_2 - g_1 (\nabla_e g_2)] \\ &\times [R_1 (\nabla_e R_2) - (\nabla_e R_1) R_2] \} . \end{aligned} \tag{B9}$$

The second integral can be carried out in the same way as the normalization integral because the Laplacian operates only on the radial part wave functions. The first and third terms can be reduced furthermore as follows. We note that for the $L=0$ exciton state g_i has a typical form of $e^{-\alpha r_{eh}} r_{eh}^n P_m(\cos\Theta_{eh})$ and can be expanded as

$$g_i(r_e, r_h) = \sum_l P_l(\cos\Theta_{eh}) \mathcal{G}_l^{(i)}(|r_e|, |r_h|) , \tag{B10}$$

using the relations in Appendix C. Here $\mathcal{G}_l$ is a function of only the radial coordinates. Making use of the relation

$$\int d\Omega_e d\Omega_h \frac{\partial}{\partial \Omega_e} P_l(\cos\Theta_{eh}) \frac{\partial}{\partial \Omega_e} P_{l'}(\cos\Theta_{eh}) = \frac{(4\pi)^2}{2l+1} l(l+1) \delta_{ll'} , \tag{B11}$$

where $\partial/\partial\Omega_e$ stands for the derivative with respect to the angular variables, we find

$$\int d\tau (\nabla_e g_1)(\nabla_e g_2) R_1 R_2 = (4\pi)^2 \int_0^R dr_e r_e^2 \int_0^R dr_h r_h^2 \left[\sum_l \frac{1}{2l+1} \frac{\partial \mathcal{G}_l^{(1)}}{\partial r_e} \frac{\partial \mathcal{G}_l^{(2)}}{\partial r_e} + \frac{1}{r_e^2} \sum_l \frac{l(l+1)}{2l+1} \mathcal{G}_l^{(1)} \mathcal{G}_l^{(2)} \right] R_1 R_2 \tag{B12}$$

and

$$\begin{aligned} \int d\tau [(\nabla_e g_1) g_2 - g_1 (\nabla_e g_2)][R_1 (\nabla_e R_2) - (\nabla_e R_1) R_2] \\ = (4\pi)^2 \int_0^R dr_e r_e^2 \int_0^R dr_h r_h^2 \sum_l \frac{1}{2l+1} \left[\frac{\partial \mathcal{G}_l^{(1)}}{\partial r_e} \mathcal{G}_l^{(2)} - \mathcal{G}_l^{(1)} \frac{\partial \mathcal{G}_l^{(2)}}{\partial r_e} \right] \left[R_1 \frac{\partial R_2}{\partial r_e} - \frac{\partial R_1}{\partial r_e} R_2 \right] . \end{aligned} \tag{B13}$$

The function $\mathcal{G}_l^{(i)}$ is a linear combination of the functions $\{G_l^{(n)}(r_e, r_h)\}$. In this way all terms in (B9) are reduced to radial integrals.

APPENDIX C: EXPRESSION OF $G_l^{(n)}(r_e, r_h, a)$

Here the expression of $G_l^{(n)}(r_e, r_h, a)$ defined by (B4) will be presented. The integration over k can be performed by a contour integral and we have, for example,

$$G_l^{(-1)}(r_e, r_h, a) = -\frac{a}{4\pi} h_l^{(1)}(iar_>) j_l(iar_<) , \tag{C1}$$

where $r_> = \max(r_e, r_h)$, $r_< = \min(r_e, r_h)$, and $h_l^{(1)}$ is the spherical Hankel function of the first kind. Then $G_l^{(n)}$ can be obtained by successive differentiation with respect to a. It is convenient to rewrite the spherical Bessel and Hankel functions for pure imaginary arguments in terms of real functions defined for $n = 0, 1, 2, \ldots$ by[58]

$$\begin{aligned} \frac{d^n}{d(ix)^n} j_l(ix) &= (2ix)^{l-n} \mathcal{I}_l^{(n)}(x) , \\ \frac{d^n}{d(ix)^n} h_l^{(1)}(ix) &= i \mathcal{H}_l^{(n)}(x) / (2ix)^{l+1+n} . \end{aligned} \tag{C2}$$

Then we have

$$G_l^{(-1)}(r_e, r_h, a) = -\frac{1}{8\pi} \frac{r_<^l}{r_>^{l+1}} \mathcal{H}_l^{(0)}(ar_>) \mathcal{I}_l^{(0)}(ar_<) \tag{C3}$$

and

$$G_l^{(n)}(r_e, r_h, a) = \frac{(-1)^n}{4\pi (2a)^{n+1}} \frac{r_<^l}{r_>^{l+1}} \left[(n+1) \sum_{r=0}^{n} {}_nC_r \mathcal{H}_l^{(r)}(ar_>) \mathcal{I}_l^{(n-r)}(ar_<) + \tfrac{1}{2} \sum_{r=0}^{n+1} {}_{n+1}C_r \mathcal{H}_l^{(r)}(ar_>) \mathcal{I}_l^{(n+1-r)}(ar_<) \right] , \tag{C4}$$

where $n \geq 0$ and ${}_nC_r$ is a binomial coefficient.

APPENDIX D: EXCITON OSCILLATOR STRENGTH AND SHORT-RANGE EXCHANGE ENERGY IN THE LIMIT OF $R \to 0$

Here the asymptotic behaviors of the oscillator strength and the short-range electron-hole exchange energy of the lowest-energy exciton state are examined in the limit of vanishing crystallite radius, i.e., $R \to 0$. In this limit the exciton envelope function can be approximated by (2.12). The normalization constant is determined by

$$\frac{C_\Phi^2(4\pi)^3R^6}{v_0^2(k_1^0)^6}\int_0^\pi dx_e x_e^2 j_0^2(x_e)\int_0^\pi dx_h x_h^2 j_0^2(x_h)G_0^{(0)}(x_e,x_h,2\alpha R/k_1^0)=1 , \tag{D1}$$

with

$$G_0^{(0)}(x_e,x_h,a)\equiv\int_0^\infty dk\, k^2\frac{a}{\pi^2(k^2+a^2)^2}j_0(kx_e)j_0(kx_h)$$

$$=\frac{e^{-ax_>}}{8\pi a^2 x_> x_<}[(ax_>-ax_<+1)e^{ax_<}-(ax_>+ax_<+1)e^{-ax_<}] , \tag{D2}$$

where $x_> = \max(x_e,x_h)$, $x_< = \min(x_e,x_h)$, and v_0 is the volume of a unit cell. In the limit of $R \to 0$, $2\alpha R/k_1^0$ approaches zero and $G_0^{(0)}(x_e,x_h,2\alpha R/k_1^0)$ takes a value of $1/(4\pi)$. Then we find

$$C_\Phi=\frac{v_0(k_1^0)^3}{2\pi^2R^3} . \tag{D3}$$

The enhancement factor of the oscillator strength in (6.5) is given by a square of

$$\sum_r \Phi(r,r)=C_\Phi\sum_r j_0^2\left[k_1^0\frac{r}{R}\right]=\frac{2\pi^2C_\Phi R^3}{v_0(k_1^0)^3} . \tag{D4}$$

Substituting the expression of C_Φ into (D4), we have

$$f_X/f_0=|\sum_r \Phi(r,r)|^2=1 . \tag{D5}$$

Thus in the limit of $R \to 0$, the oscillator strength of the lowest-energy exciton in a quantum dot approaches that of the band-to-band transition in the bulk material.

On the other hand, the enhancement factor of the short-range part of the electron-hole exchange energy is given by (8.7) and is proportional to

$$\sum_r |\Phi(r,r)|^2=C_\Phi^2\sum_r j_0^4\left[k_1^0\frac{r}{R}\right]$$

$$=\frac{4\pi C_\Phi^2R^3}{v_0(k_1^0)^3}[\mathrm{Si}(2\pi)-\tfrac{1}{2}\mathrm{Si}(4\pi)] , \tag{D6}$$

where Si is the sine integral function. Substituting the expression of C_Φ into (D6), we obtain

$$\sum_r|\Phi(r,r)|^2=\frac{v_0}{R^3}[\mathrm{Si}(2\pi)-\tfrac{1}{2}\mathrm{Si}(4\pi)]\cong 0.672\frac{v_0}{R^3} . \tag{D7}$$

Thus the short-range part of the exchange energy shows an increase proportional to R^{-3} in the limit of $R \to 0$.

APPENDIX E: ELECTRON-HOLE EXCHANGE INTERACTION IN THE SITE REPRESENTATION

The electron-hole exchange interaction is usually derived in the Bloch orbital representation. However, in the case of quantum dot, the site or Wannier orbital representation is more desirable because the wave vector is not well defined due to the three-dimensional confinement. Here we will derive the electron-hole exchange interaction in the site representation. An excitonic state in the site representation is written as

$$|\Phi_\lambda\rangle=\sum_{\nu\tau r_e}\sum_{\mu\sigma r_h}\Phi^\lambda_{\nu\tau,\mu\sigma}(r_e,r_h)a^\dagger_{\nu\tau r_e}a_{\mu\sigma r_h}|0\rangle , \tag{E1}$$

where $a(a^\dagger)$ is the annihilation (creation) operator in the site representation and $|0\rangle$ denotes the ground state of the system, and the eigenvalue equation for the envelope function $\Phi^\lambda_{\nu\tau,\mu\sigma}(r_e,r_h)$ is given by

$$\sum_{\nu'\tau'r_e'}\sum_{\mu'\sigma'r_h'}H_{\{\nu\tau r_e,\mu\sigma r_h\}\{\nu'\tau'r_e',\mu'\sigma'r_h'\}}\Phi^\lambda_{\nu'\tau',\mu'\sigma'}(r_e',r_h')$$

$$=\epsilon_\lambda\Phi^\lambda_{\nu\tau,\mu\sigma}(r_e,r_h) \tag{E2}$$

with

$$H_{\{\nu\tau r_e,\mu\sigma r_h\}\{\nu'\tau'r_e',\mu'\sigma'r_h'\}}$$

$$=\langle 0|a^\dagger_{\mu\sigma r_h}a_{\nu\tau r_e}[H,a^\dagger_{\nu'\tau'r_e'}a_{\mu'\sigma'r_h'}]|0\rangle , \tag{E3}$$

where (μ,μ') and (ν,ν') stand for the indices of the valence and conduction bands, respectively, (σ,σ') and (τ,τ') are the spin indices of the respective band states, ϵ_λ is the excitation energy relative to the ground state of the system, and H is the relevant Hamiltonian. The electron-hole exchange term in (E3) is found to be $V(\nu\tau r_e,\mu'\sigma'r_h';\nu'\tau'r_e',\mu\sigma r_h)$ with the definition

$$V(\lambda_1\sigma_1r_1,\lambda_2\sigma_2r_2;\lambda_3\sigma_3r_3,\lambda_4\sigma_4r_4)$$

$$\equiv\int d^3r\int d^3r'\phi^*_{\lambda_1\sigma_1r_1}(r)\phi^*_{\lambda_2\sigma_2r_2}(r')V(r-r')\phi_{\lambda_3\sigma_3r_3}(r')$$

$$\times\phi_{\lambda_4\sigma_4r_4}(r) , \tag{E4}$$

where $\phi_{\lambda_i\sigma_ir_i}$ is a Wannier orbital belonging to the λ_i band with the spin state σ_i which is localized at the site r_i and $V(r-r')$ is the Coulomb potential. Then the electron-hole exchange energy of the λ exciton state is calculated as

$$\sum_{\nu\tau r_e}\sum_{\mu\sigma r_h}\sum_{\nu'\tau'r_e'}\sum_{\mu'\sigma'r_h'}\Phi^{\lambda*}_{\nu\tau,\mu\sigma}(r_e,r_h)\Phi^\lambda_{\nu'\tau',\mu'\sigma'}(r_e',r_h')$$

$$\times V(\nu\tau r_e,\mu'\sigma'r_h';\nu'\tau'r_e',\mu\sigma r_h) . \tag{E5}$$

[1]A. I. Ekimov, Al. L. Efros, and A. A. Onushchenko, Solid State Commun. **56**, 921 (1985).
[2]N. F. Borrelli, D. W. Hall, H. J. Holland, and D. W. Smith, J. Appl. Phys. **61**, 5399 (1987).
[3]T. Itoh, Y. Iwabuchi, and M. Kataoka, Phys. Status Solidi B **145**, 567 (1988); T. Itoh, Y. Iwabuchi, and T. Kirihara, *ibid.* **146**, 531 (1988).
[4]L. E. Brus, IEEE J. Quantum Electron. **QE-22**, 1909 (1986).
[5]Y. Wang, N. Herron, W. Mahler, and A. Suna, J. Opt. Soc. Am. B **6**, 808 (1989).
[6]K. Kash, A. Scherer, J. M. Worlock, H. G. Craighead, and M. C. Tamargo, Appl. Phys. Lett. **49**, 1043 (1986).
[7]J. Cibert, P. M. Petroff, G. J. Dolan, S. J. Pearton, A. C. Gossard, and J. H. English, Appl. Phys. Lett. **49**, 1275 (1986).
[8]Y. Miyamoto, M. Cao, Y. Shingai, K. Furuya, Y. Suematsu, K. G. Ravikumar, and S. Arai, Jpn. J. Appl. Phys. **26**, L225 (1987).
[9]See, for example, the review by D. Heitmann, K. Kern, T. Demel, P. Grambow, K. Ploog, and Y. H. Zhang, Surf. Sci. **267**, 245 (1992).
[10]T. Fukui, S. Ando, Y. Tokura, and T. Toriyama, Appl. Phys. Lett. **58**, 2018 (1991).
[11]J. A. Lebens, C. S. Tsai, K. J. Vahala, and T. F. Kuech, Appl. Phys. Lett. **56**, 2642 (1990).
[12]A. I. Ekimov and A. A. Onushchenko, Fiz. Tekh. Poluprovodn. **16**, 1215 (1982) [Sov. Phys. Semicond. **16**, 775 (1982)].
[13]R. K. Jain and R. C. Lind, J. Opt. Soc. Am. **73**, 647 (1983).
[14]N. Chestnoy, T. D. Harris, R. Hull, and L. E. Brus, J. Phys. Chem. **90**, 3393 (1986).
[15]M. G. Bawendi, W. L. Wilson, L. Rothberg, P. J. Carroll, T. M. Jedju, M. L. Steigerwald, and L. E. Brus, Phys. Rev. Lett. **65**, 1623 (1990).
[16]P. Roussignol, D. Ricard, J. Lukasik, and C. Flytzanis, J. Opt. Soc. Am. B **4**, 5 (1987).
[17]P. Roussignol, D. Ricard, and C. Flytzanis, Appl. Phys. A **44**, 285 (1987).
[18]P. Roussignol, D. Ricard, C. Flytzanis, and N. Neuroth, Phys. Rev. Lett. **62**, 312 (1989).
[19]G. R. Olbright and N. Peyghambarian, Appl. Phys. Lett. **48**, 1184 (1986).
[20]S. H. Park, R. A. Morgan, Y. Z. Hu, M. Lindberg, S. W. Koch, and N. Peyghambarian, J. Opt. Soc. Am. B **7**, 2097 (1990).
[21]H. Weller, H. M. Schmidt, U. Koch, A. Fojtik, S. Baral, A. Henglein, W. Kunath, K. Weiss, and E. Diemann, Chem. Phys. Lett. **124**, 557 (1986).
[22]J. Yumoto, S. Fukushima, and K. Kubodera, Opt. Lett. **12**, 832 (1987).
[23]H. Shinojima, J. Yumoto, N. Uesugi, S. Omi, and Y. Asahara, Appl. Phys. Lett. **55**, 1519 (1989).
[24]Y. Masumoto, M. Yamazaki, and H. Sugawara, Appl. Phys. Lett. **53**, 1527 (1988).
[25]A. Nakamura, H. Yamada, and T. Tokizaki, Phys. Rev. B **40**, 8585 (1989).
[26]T. Itoh, T. Ikehara, and Y. Iwabuchi, J. Lumin. **45**, 29 (1990).
[27]T. Takagahara, Phys. Rev. B **36**, 9293 (1987).
[28]E. Hanamura, Phys. Rev. B **37**, 1273 (1988).
[29]L. V. Keldysh, Pis'ma Zh. Eksp. Teor. Fiz. **29**, 716 (1979) [JETP Lett. **29**, 658 (1979)]; Superlatt. Microstruct. **4**, 637 (1988).
[30]M. Kumagai, and T. Takagahara, Phys. Rev. B **40**, 12 359 (1989).
[31]L. Banyai, I. Galbraith, C. Ell, and H. Haug, Phys. Rev. B **36**, 6099 (1987).
[32]T. Ogawa and T. Takagahara, Phys. Rev. B **44**, 8138 (1991).
[33]R. S. Knox, *Solid State Physics,* edited by F. Seitz and D. Turnbull (Academic, New York, 1963), Suppl. No. 5.
[34]Al. L. Efros and A. L. Efros, Fiz. Tekh. Poluprovodn. **16**, 1209 (1982) [Sov. Phys.-Semicond. **16**, 772 (1982)].
[35]L. E. Brus, J. Chem. Phys. **80**, 4403 (1984).
[36]H. M. Schmidt and H. Weller, Chem. Phys. Lett. **129**, 615 (1986).
[37]S. V. Nair, S. Sinha, and K. C. Rustagi, Phys. Rev. B **35**, 4098 (1987).
[38]Y. Kayanuma, Phys. Rev. B **38**, 9797 (1988).
[39]J. B. Xia, Phys. Rev. B **40**, 8500 (1989).
[40]P. E. Lippens and M. Lannoo, Phys. Rev. B **39**, 10 935 (1989).
[41]Y. Z. Hu, M. Lindberg, and S. W. Koch, Phys. Rev. B **42**, 1713 (1990).
[42]P. C. Sercel and K. J. Vahala, Phys. Rev. B **42**, 3690 (1990).
[43]Y. Kayanuma and H. Momiji, Phys. Rev. B **41**, 10 261 (1990).
[44]D. B. Tran Thoai, Y. Z. Hu, and S. W. Koch, Phys. Rev. B **42**, 11 261 (1990).
[45]E. A. Hylleraas, Z. Phys. **54**, 347 (1929).
[46]D. Ahn and S. L. Chuang, Appl. Phys. Lett. **49**, 1450 (1986).
[47]R. Bauer, D. Bimberg, J. Christen, D. Oertel, D. Mars, J. N. Miller, T. Fukunaga, and H. Nakashima, in *Proceedings of the 18th International Conference on Semiconductor Physics,* edited by O. Engström (World-Scientific, Singapore, 1987), p. 525.
[48]M. Potemski, J. C. Maan, A. Fasolino, K. Ploog, and G. Weimann, Surf. Sci. **229**, 151 (1990).
[49]Y. Chen, B. Gil, P. Lefebvre, and H. Mathieu, Phys. Rev. B **37**, 6429 (1988).
[50]L. C. Andreani and F. Bassani, Phys. Rev. B **41**, 7536 (1990).
[51]U. Rössler, S. Jorda, and D. Broido, Solid State Commun. **73**, 209 (1990).
[52]Y. Onodera and Y. Toyozawa, J. Phys. Soc. Jpn. **22**, 833 (1967).
[53]W. Staude, Phys. Status Solidi B **43**, 367 (1971). In the author's notation, $\Delta_{TR}=\Delta_{ex}-\Delta_{dip}$ and $\Delta_L=\Delta_{ex}+2\Delta_{dip}$. Using the values $\Delta_{TR}=8.7$ meV and $\Delta_{LT}=3\Delta_{dip}=5.4$ meV, obtain $\Delta_{ex}=10.5$ meV and $\Delta_{dip}=1.8$ meV.
[54]R. G. Ulbrich and C. Weisbuch, Phys. Rev. Lett. **38**, 865 (1977).
[55]W. Ekardt, K. Lösch, and D. Bimberg, Phys. Rev. B **20**, 3303 (1979).
[56]S. Schmitt-Rink, D. A. B. Miller, and D. S. Chemla, Phys. Rev. B **35**, 8113 (1987).
[57]T. Takagahara, in *Ultrafast Phenomena VI,* edited by T. Yajima, K. Yoshihara, C. B. Harris, and S. Shionoya (Springer, Berlin, 1988), p. 337.
[58]A minor change is made on the previous notation [T. Takagahara, Phys. Rev. B **39**, 10 206 (1989)]; namely, $J_l^R(H_l^R)$ is denoted here by $\mathscr{J}_l(\mathscr{H}_l)$.